RBRH

Revista Brasileira de Recursos Hídricos
Brazilian Journal of Water Resources
Versão On-line ISSN 2318-0331
RBRH, Porto Alegre, v. 28, e19, 2023
Technical Note

https://doi.org/10.1590/2318-0331.282320230005

Evaluation of shear rate formulations through steady uniform non-Newtonian fluid flows in the context of shallow-water equations

Avaliação de formulações de taxa de deformação através de escoamentos permanentes e uniformes de fluidos não-Newtonianos no contexto de equações de águas rasas

Yuri Taglieri Sáo[1], João Batista Pereira[1] & Geraldo de Freitas Maciel[1]

[1]Universidade Estadual Paulista "Júlio de Mesquita Filho", Ilha Solteira, SP, Brasil
E-mails: yuri.sao@unesp.br (YTS), jbpereira.eng@gmail.com (JBP), geraldo.f.maciel@unesp.br (GFM)

Received: January 13, 2023 - Revised: April 26, 2023 - Accepted: May 09, 2023

ABSTRACT

Non-Newtonian rheology effects, such as pseudoplasticity and viscoplasticity, are understood as shear stresses, incorporated to the energy slope term in the Shallow-Water Equations (SWE). However, non-Newtonian shear stresses are dependent of the shear rate, whose formulation is a function of the gradient of the velocity profile in the bottom. This study investigated two shear rate formulations that are commonly applied in the SWE literature: 1) a non-parameterized function; and 2) a function based on the Herschel-Bulkley rheological model. Their influence in steady uniform flows of non-Newtonian fluids was evaluated through numerical-theoretical comparisons. A Lax-Friedrichs scheme was implemented to solve the SWE system and allowed employing the shear rate formulations. Experimental tests were carried out and numerical simulations of hypothetical scenarios were performed. It was found that the non-parameterized formulation presented deviation in normal depth up to 14% in comparison with theoretical solution, while the formulation based on the Herschel-Bulkley model provided a good agreement, corroborated by punctual Computational Fluid Dynamics simulations (deviation less than 2%) and experimental data. The ratio of both shear rate formulations is strongly correlated to the deviation of normal depth, indicating that the non-parameterized shear rate function does not provide an acceptable result in the steady uniform flow.

Keywords: Shallow-water equations; HEC-RAS; Non-Newtonian fluid.

RESUMO

Efeitos de reologia não-Newtoniana, como pseudoplasticidade e viscoplasticidade, são interpretados como tensões cisalhantes, incorporados à declividade da linha de energia nas Equações de Águas Rasas. Entretanto, tensões de cisalhamento devido a efeitos não-Newtonianos são dependentes da taxa de deformação, cuja formulação é função do gradiente do perfil de velocidade no fundo do canal. No contexto do sistema de Equações de Águas Rasas, este estudo investigou duas formulações de taxa de deformação comumente empregadas na literatura: a primeira é uma função não-parametrizada e a segunda é uma função baseada no modelo reológico de Herschel-Bulkley. A influência dessas formulações em escoamentos permanentes e uniformes idealizados de fluidos não-Newtonianos foi avaliada através de comparações numéricas e teóricas. O esquema Lax-Friedrichs de diferenças finitas foi implementado para resolver o sistema de Equações de Águas Rasas e permitiu empregar as formulações de taxa de deformação. Várias simulações numéricas de cenários hipotéticos e casos experimentais foram executadas. Observou-se que a formulação não-parametrizada apresentou desvios na solução da lâmina normal até 14% em comparação com a solução teórica, enquanto que a formulação baseada no modelo de Herschel-Bulkley forneceu uma boa confrontação, corroborada por simulações pontuais de Fluidodinâmica Computacional (desvio de menos de 2%) e dados experimentais. A razão entre ambas formulações está fortemente correlacionada com o desvio na solução da lâmina normal, o que indica que a formulação não-parametrizada de taxa de deformação não produz resultados aceitáveis em escoamentos permanentes e uniformes.

Palavras-chave: Equações de águas rasas; HEC-RAS; Fluido não-Newtoniano.

INTRODUCTION

Natural hazards and disasters, such as mudflows, debris flows and tailings dam-breaks, are capable of transporting highly concentrated materials, whose physical properties are considered to be non-Newtonian in a hydraulics point-of-view (Jing et al., 2018; Coussot & Piau, 1994; Coussot et al., 1998). Disasters such as occurred in Mount Polley-BC (Canada/2014), Mariana-MG (Brazil/2015) and Brumadinho-MG (Brazil/2019) made the stakeholders (government, mining companies and engineers) take action and study methods to prevent, mitigate and elaborate better emergency plans (Martin et al., 2019; Gildeh et al., 2021). In Brazil, new legislations, such as the Resolution number 95, from February 7th 2022, were approved by the Agência Nacional de Mineração (ANM) to improve the emergency plans in dam-break cases, demanding the inclusion of studies such as geotechnical and rheological characterization of tailings. Thus, the scientific community has been increasing its interest to study non-Newtonian hydraulics.

Commonly, these hazardous flows are modelled by the Shallow-Water Equations (SWE) system, which applies both to Newtonian and non-Newtonian flows (Tan, 1992; Castro-Orgaz & Hager, 2019). In classical hydraulics, the SWE system is used to study flood routing, water dam-break, wave propagation, among many other applications (Tsakiris & Bellos, 2014; Fraccarollo & Toro, 1995; Liang et al., 2006; Hu et al., 2000). The literature and engineering practice often use widely recognized numerical codes that solve the SWE system, such as FLO-2D and HEC-RAS, due to their capability of working along with topographic data, to optimized computational performance and tools able to solve many engineering problems (Hicks & Peacock, 2005; Yi, 2011; Wu et al., 2013; O'Brien et al., 1993). A documental analysis of tailings dam-break studies for emergency plans in the state of Minas Gerais, Brazil, for example, stated that almost all studies were carried out with either one of these numerical codes (Paiva et al., 2020).

To include non-Newtonian effects into the SWE system, the most common approach is to add non-Newtonian shear stresses to the friction term (Ancey et al., 2012) along with other sources of stresses, such as turbulence and grain interaction (O'Brien et al., 1993). While non-Newtonian effect of viscoplasticity (yield stress) is included straightforwardly, the viscous shear stress is dependent on the shear rate. The shear rate formulation is obtained through estimates from the vertical velocity profile (Iverson, 1997) and two approaches are found in the literature. One considers a non-parameterized parabolic velocity profile in the vertical direction, resulting in a simple function of mean velocity and flow depth (O'Brien et al., 1993; Gibson et al., 2021; Gibson et al., 2022). The other considers the analytical solution of the velocity profile in the vertical direction, resulting in shear rate dependent of rheological parameters of the fluid, mean velocity and depth (Boutounet et al., 2016; Huang & Garcia, 1998; Di Cristo et al., 2013).

This study aims to investigate both shear rate formulations employed in literature through the steady uniform flow over an inclined rectangular open channel for Newtonian and non-Newtonian fluids, limiting itself to fluids without thermal and viscoelasticity dependencies. This case has a well-established theoretical solution based on Shallow-Water hypothesis (Coussot, 1994), thus it can be used as a reference to evaluate numerical simulations results.

It is important to notice that the steady uniform flow is used only as a reference case, since geophysical and hazardous flows are commonly unsteady and non-uniform (Coussot & Meunier, 1996). However, this case is useful to investigate the aforementioned shear rate formulations, since it presents a theoretical solution and there are experimental data available. Moreover, it is part of basic scientific research of numerical models, functioning as a benchmark test before simulating cases of non-Newtonian flows that are more complex, such as tailings dam-breaks and debris flows.

MATERIALS AND METHODS

In this work, the normal depth and shear rate of steady uniform flows are the main properties to be evaluated through theoretical, numerical and experimental tests. First, Subsection "Theoretical solution of steady and uniform flow over an inclined rectangular channel of non-Newtonian fluids" shows the deduction of theoretical solutions for those properties. Then, three numerical methods (Lax-Friedrichs scheme, HEC-RAS 6.3 and ANSYS Fluent 14.5) are described in Subsection "Numerical methods", followed by the description of experimental methods employed in this work in Subsection "Experimental methods". Finally, Subsection "Test scenarios" define the test scenarios to be evaluated in this study.

Theoretical solution of steady and uniform flow over an inclined rectangular channel of non-Newtonian fluids

The coordinate system is oriented as (x,z), where x is the longitudinal direction and z is the flow height direction, and the velocity field is given by (u,w) components. The fluid is considered to be incompressible, within an isothermal flow, does not present viscoelastic effects and its rheological behavior follows the Herschel-Bulkley constitutive law. Considering steady-state regime, simple shear conditions and shallow fluid layer, the shear stress is dominated by its vertical component τ_{xz}, being exclusively dependent of the shear rate $\dot{\gamma} = \partial u / \partial z$. Then, the Herschel-Bulkley constitutive law reduces to Equation 1, which depends on the yield stress τ_c, consistency index K_n and flow index n (Balmforth et al., 2007). Moreover, the Herschel-Bulkley model can recover the Bingham model ($n=1$ and $\tau_c > 0$), the Power-Law model ($n \neq 1$ and $\tau_c = 0$) and the Newtonian model ($n=1$ and $\tau_c = 0$).

$$\tau_{xz} = K_n \left| \frac{\partial u}{\partial z} \right|^{n-1} \frac{\partial u}{\partial z} + \tau_c \, sgn\left(\frac{\partial u}{\partial z} \right) \tag{1}$$

Where $\partial u / \partial z = 0$ if $|\tau_{xz}| < \tau_c$.

Note that materials transported by geophysical flows present a very complex nature, especially due to the variety of grain sizes and, consequently, to particle and interstitial fluid interactions (Iverson, 1997). A common approach is to characterize these mesoscopic-scale interactions in a macroscopic-scale point-of-view, resulting in the rheological characterization of the material (Coussot, 2017). Once the fluid is characterized adequately and carefully through rheometry techniques, the fluid mechanics/hydraulics approach can be applied, as this work does.

The governing equations are integrated considering the aforementioned hypotheses, under uniform flow and fully developed flow conditions in a rectangular and wide channel. Using the zero-shear stress at the free surface and no-slip condition at the bottom as boundary conditions, the velocity profile is given by Equation 2, which corresponds to an idealized version for mud, debris and tailings steady uniform flows (Coussot, 1994).

$$u(z)=\begin{cases}\dfrac{n}{n+1}\left[\dfrac{\rho g\sin\theta}{K_n}z_0^{n+1}\right]^{1/n}\left[1-\left(1-\dfrac{z}{z_0}\right)^{\frac{n+1}{n}}\right], & if\ 0\le z\le z_0\\ \dfrac{n}{n+1}\left[\dfrac{\rho g\sin\theta}{K_n}\right]^{1/n}, & if\ z_0<z\le h_0\end{cases} \tag{2}$$

Where h_0 is the normal depth of the flow, $z_0=h_0-\tau_c/(\rho g\sin\theta)$ is the non-sheared region (plug flow) height and u_p is the non-sheared flow velocity.

The mean value theorem is applied to Equation 2 and provides the mean velocity of the flow $\bar{U}$, given by Equation 3 (Coussot, 1994; Maciel et al., 2013). The volumetric flow rate Q can be obtained by simply multiplying $\bar{U}$ by the wetted area $A=h_0 b$, where b is the channel width. The normal depth h_0 can be implicitly calculated (e.g. a Newton-Raphson scheme) by defining the volumetric flow rate Q, Herschel-Bulkley parameters of the fluid (τ_c, K_n and n) and its density ρ, channel width b and slope θ.

$$\bar{U}=\frac{n}{n+1}\left(\frac{\rho g sin\theta}{K_n}\right)^{\frac{1}{n}}z_0^{\frac{n+1}{n}}\left[1-\frac{n}{2n+1}\left(1-C^*\right)\right] \tag{3}$$

Where $C^*=\tau_c/(\rho g h_0\sin\theta)$ is the dimensionless yield stress.

Under steady, uniform and Shallow-Water conditions, the vertically averaged shear rate is equal to the bottom shear rate $\dot{\gamma}_b$. To obtain a shear rate in function of the Herschel-Bulkley rheological parameters, mean velocity and normal depth, first the theoretical velocity profile $u(z)$ (Equation 2) is differentiated along z-direction and then evaluated at the bottom ($z=0$), resulting in Equation 4:

$$\left.\frac{du}{dz}\right|_{z=0}=\frac{1}{z_0}\left(\frac{\rho g\sin\theta z_0^{n+1}}{K_n}\right)^{\frac{1}{n}} \tag{4}$$

Then, Equation 4 is inserted in Equation 3 and, after rearrangements, the depth-averaged non-Newtonian shear rate, now called $\dot{\gamma}_{HB}$, is given by Equation 5. This shear rate formulation includes relevant fluid properties, i.e. the pseudoplasticity and the viscoplasticity through the flow index n and the yield stress τ_c within C^*, respectively. It should be noted that Equation 5 does not require additional parameters, aside from the rheological parameters, to be estimated by practitioners, since the flow index n and yield stress within C^* (Equation 3) are expected to be known (e.g. from rheometry measurements) while modelling Herschel-Bulkley fluid flows.

$$\dot{\gamma}_{HB}=\frac{n+1}{n\left(1-C^*\right)^2\left(\dfrac{1}{1-C^*}-\dfrac{n}{2n+1}\right)}\frac{\bar{U}}{h_0} \tag{5}$$

Similar developments were made by Ng & Mei (1994) and Di Cristo et al. (2013) for power-law fluids ($n\neq1$ and $C^*=0$) and by Huang & Garcia (1998) and Boutounet et al. (2016) for Herschel-Bulkley fluids ($n\neq1$ and $C^*>0$). Note that for a Newtonian fluid ($n=1$ and $C^*=0$), the well-known expression for the non-parameterized shear rate $\dot{\gamma}_N$, function of only mean velocity and depth (O'Brien et al., 1993; Iverson, 1997; Gibson et al., 2021), is recovered, given by Equation 6. The subscript "$_N$" refers to "Newtonian". Other authors (Jeyapalan et al., 1983) use the constant "2" instead of "3", considering a parabolic distribution with maximum velocity.

$$\dot{\gamma}_N=\frac{3\bar{U}}{h_0} \tag{6}$$

Numerical methods

Mathematical model: the Shallow-Water Equations (SWE)

The Shallow-Water Equations (SWE) are widely used to model free surface flows where the vertical length scale is significantly smaller than the horizontal length scale (Castro-Orgaz & Hager, 2019). Physically, they express the conservation of mass and momentum along the flow and can describe one or two-dimensional flows, since the SWE neglect the vertical velocity and assume that the distribution of velocity in each section is uniform (Castro-Orgaz & Hager, 2019). To model a flow using the SWE, some hypotheses must be considered: pressure distribution is hydrostatic; the slope of the channel is small; internal shear stresses are negligible in comparison of friction at the bottom; and formulas from the steady uniform flow can be used to compute the friction stress (i.e. Manning-Chézy-Strickler, Hazen-Williams, among others) (Tan, 1992; Castro-Orgaz & Hager, 2019).

The one-dimensional SWE system can be written in conservative form (Garcia-Navarro et al., 1992; Gama et al., 2020) and in function of wetted area A and volumetric flow rate Q, as showed by Equation 7 and by its components in Equations 8a, 8b and 8c.

$$\frac{\partial \boldsymbol{q}}{\partial t}+\frac{\partial \boldsymbol{f}}{\partial x}=\boldsymbol{J} \tag{7}$$

Where

$$\boldsymbol{q}=\begin{bmatrix}A\\ Q\end{bmatrix} \tag{8a}$$

$$\boldsymbol{f}=\begin{bmatrix}Q\\ \dfrac{Q^2}{A}+gA\bar{h}\cos\theta\end{bmatrix} \tag{8b}$$

$$\boldsymbol{J}=\begin{bmatrix}0\\ gAS_0-gAS_f\end{bmatrix} \tag{8c}$$

Where $\boldsymbol{q}$ is the vector of time-dependent terms, $\boldsymbol{f}$ is the vector of space-dependent terms, $\boldsymbol{J}$ is the source term vector, $\bar{h}$ is the depth of the center of gravity of the cross section, S_0 is the channel slope and S_f the energy slope due to friction effects.

Lax-Friedrichs finite difference scheme

The first numerical code used in this work to discretize the SWE system is the Lax-Friedrichs (LF) finite difference scheme (Gama et al., 2020). It allows implementing different bottom friction terms into the source term $\boldsymbol{J}$ and solving numerically the one-dimensional SWE. This scheme is explicit and first order in both space and time. Even though it is a first order scheme, its accuracy is considered to be sufficient to the methodology of this work, since there are no shocks and/or discontinuities in the solution for steady uniform flow. A Total Variation Diminishing (TVD) second-order scheme, (e.g. TVD-MacCormack scheme (Garcia-Navarro et al., 1992), the MUSCL scheme (Van Leer, 1979), among others) would be required if shock-capturing properties were necessary to the work.

The code was implemented in Python language, using the Jupyter Notebook interface. To solve numerically Equation 7 through the LF scheme, the domain is discretized as $x_i = i\Delta x$ in space and $t^n = n\Delta t$ in time, where Δx and Δt are the grid size and time step, respectively. The spatial domain $L = 10m$ is discretized uniformly in 300 cells, whereas the time step is variable and calculated based on the Courant Number C, given by Equation 9. The Courant Number is used as stability criteria and must be lower than 1.0 to guarantee stability. Time step Δt is calculated for each cell fixing Courant Number as 0.25 and the smaller time step is chosen for the simulation. A constant flow rate is imposed as boundary condition for the first cell (upstream) and an order-zero extrapolation is applied to the last cell (downstream).

$$C = \Delta t \frac{|V| + \sqrt{gh}}{\Delta x} \tag{9}$$

Where $|V|$ is the velocity magnitude of the cell and h is the local depth in the cell.

The values of vectors $\boldsymbol{q}$ and $\boldsymbol{f}$ can be computed in the subsequent time step for each internal cell through Equation 10.

$$\boldsymbol{q}_i^{n+1} = \frac{1}{2}\left(\boldsymbol{q}_{i+1}^n + \boldsymbol{q}_{i-1}^n\right) - \frac{\Delta t}{2\Delta x}\left[\boldsymbol{f}(\boldsymbol{q})_{i+1}^n - \boldsymbol{f}(\boldsymbol{q})_{i-1}^n\right] + \Delta t \frac{\boldsymbol{J}_{i+1}^n + \boldsymbol{J}_{i-1}^n}{2} \tag{10}$$

Two equations of S_f were implemented in the LF scheme. The first one (Equation 11) is based on the HEC-RAS 6.3 code (Gibson et al., 2021) and the work of O'Brien et al. (1993). Its first term considers the roughness effect in turbulent flow and its last term uses Equation 6 to model the shear rate. In the context of this work, this version of the LF numerical code is called "LF_N model", where the subscript "$_N$" refers to a Newtonian formulation of the shear rate.

$$S_f = \frac{\eta^2 Q^2}{A^2 R_h^{4/3}} + \frac{1}{\rho g h}\left(\tau_c + K_n\left(\dot{\gamma}_N\right)^n\right) \tag{11}$$

Where η is the Manning coefficient and R_h is the hydraulic radius.

The second version employs Equation 12 and uses Equation 5, incorporating both the pseudoplasticity and viscoplasticity effects into the shear rate. This version of the LF numerical code is called "LF_{HB}", where the subscript "$_{HB}$" refers to a formulation of the shear rate based on the Herschel-Bulkley rheological model.

$$S_f = \frac{1}{\rho g h}\left(\tau_c + K_n\left(\dot{\gamma}_{HB}\right)^n\right) \tag{12}$$

In total, 159 hypothetical scenarios and 31 experimental cases were simulated by both LF_N and LF_{HB} models. The scenarios and cases are described in Subsection "Test scenarios". The codes are available in .py format in the Supplementary Material.

Numerical setup employed by HEC-RAS 6.3

The second numerical code used in this work is the HEC-RAS 6.3 and it is the benchmark code to verify the correct implementation of the LF scheme. The code models one-dimensional (1D) or two-dimensional (2D) flows by solving the Shallow-Water Equations (SWE) using the Finite Volume Method [HEC-RAS Hydraulic Reference Manual 2022; US Army Corps of Engineers (2022)]. Neglecting Coriolis effects, variation of bottom topography and tangential stresses due to moving eddies, the code solves the SWE presented in Equations 7, 8a, 8b and 8c and employs Equation 11 to model the friction term.

The attribution of geometry, boundary conditions and mesh discretization was made in the HEC-RAS 6.3 environment through the Geometric Data editor and RAS Mapper, using the same procedure described in HEC-RAS Guides and Tutorials [HEC-RAS Guides and Tutorials, 2020; US Army Corps of Engineers (2020)]. A channel of $20m$ long and $0.3m$ wide was used as computational domain in order to establish a uniform flow, whose slope depends on the studied case. A constant flow rate is imposed as upstream boundary condition and the channel slope value is prescribed as downstream boundary condition.

The computational domain was discretized using a rectangular mesh of $0.03 \times 0.03m$, resulting in approximately 6660 cells, validated by the Grid Convergence Index (GCI) procedure (Celik et al., 2008) with uncertainty of 0.41% over the normal depth. Manning's roughness coefficient was subjected to sensitivity tests and $n = 0.001 s m^{-1/3}$ was sufficiently low to avoid roughness effects and to enable the comparison with the theoretical model. Time-step size was governed by the Courant-Friedrichs-Lewy (CFL) condition, which must be less than one to guarantee numerical stability. No significant effects were observed in the CFL condition sensitivity tests. Simulation time was sufficient to establish steady regime (~ 5 minutes of simulated time).

From the 159 hypothetical scenarios in total, 108 scenarios were simulated by the HEC-RAS 6.3 code. The results were then compared to results of the LF_N model in order to validate the implementation of Lax-Friedrichs schemes. The scenarios are described in Subsection "Test scenarios".

Mathematical model and numerical setup employed by ANSYS Fluent 14.5

The third numerical code used in this work is the ANSYS Fluent 14.5, a numerical code that employs the Finite Volume Method to solve Computational Fluid Dynamics problems. Differently from the LF scheme and HEC-RAS 6.3, this numerical code solves the full-momentum equations (Equations 13 and 14) instead of solving the SWE system.

Consequently, the shear rate calculation (Equation 15) is based on the complete velocity field, while SWE solvers use only mean velocity and flow depth to calculate the shear rate. Thus, it provides a third different approach to confront numerical results and evaluate the influence of shear rate formulation of SWE solvers. However, its computational cost prevents to simulate several cases, while SWE solvers, such as HEC-RAS 6.3, present significantly lower computational cost.

$$\frac{\partial \rho}{\partial t} + \vec{\nabla} \cdot \left(\rho \vec{V} \right) = 0 \tag{13}$$

$$\frac{\partial}{\partial t}\left(\rho \vec{V} \right) + \vec{\nabla} \cdot \left(\rho \vec{V} \vec{V} \right) = \rho \vec{g} - \vec{\nabla} p + \vec{\nabla} \cdot \bar{\bar{\tau}} \tag{14}$$

Where ρ is the fluid density, $\vec{V} = (u, w)$ is the velocity field and its components, and p is the pressure.

In these conditions, the shear rate $\dot{\gamma}$ is given by Equation 15.

$$\dot{\gamma} = \sqrt{\frac{1}{2} D_{ij} : D_{ij}} \tag{15}$$

Where $D_{ij} = \left(\frac{\partial u_i}{\partial x_j} + \frac{\partial u_j}{\partial x_i} \right)$.

The Volume-of-Fluid (VoF) method (Hirt & Nichols, 1981; ANSYS Fluent, 2012) is employed to track the free surface between phases (air and test-fluid), where the free surface is located at volume fraction variable $\alpha = 0.5$. Due to discontinuity in the apparent viscosity function η of viscoplastic fluid flows, a bi-viscous viscosity regularization technique (Pereira et al., 2022) is employed (Equation 16), where the critical shear rate $\dot{\gamma}_c = 0.01 s^{-1}$ is sufficiently low to adequately model the apparent viscosity function.

$$\eta(\dot{\gamma}) = \begin{cases} \dfrac{\tau_c}{\dot{\gamma}_c}\left(2 - \dfrac{\dot{\gamma}}{\dot{\gamma}_c}\right) + K_n \dot{\gamma}_c^{n-1}\left[(2-n) + (n-1)\dfrac{\dot{\gamma}}{\dot{\gamma}_c}\right], & \text{if } \dot{\gamma} \le \dot{\gamma}_c \\ \dfrac{\tau_c}{\dot{\gamma}}\left(1 + \dfrac{K_n \dot{\gamma}^n}{\tau_c}\right), & \text{if } \dot{\gamma} > \dot{\gamma}_c \end{cases} \tag{16}$$

Inlet and outlet boundary conditions were modelled as prescribed velocity (theoretical mean velocity) and atmospheric pressure/free outlet, respectively. The mesh contains 32000 finite volume cells and a very fine refinement was employed from the bottom to the predicted free surface height; spatial discretization uncertainty of $1.86\,\%$ was obtained from the GCI procedure. The SIMPLEC algorithm was employed to iteratively solve pressure and velocity variables. Unsteady regime was considered due to the usage of VoF method, time-step size was governed by the CFL condition, which was kept at a maximum of 0.25, and simulation time was sufficient to establish steady regime. Values of normal depth and shear rate at the bottom were evaluated. The study cases are described in Subsection "Test scenarios".

Experimental methods

An experimental apparatus consisting of a rectangular channel of width $b = 0.3 m$ coupled to a recirculation system was used to generate and to measure normal depth of steady uniform flows. The experimental apparatus has been used in previous experimental runs (Fiorot et al., 2015; Maciel et al., 2017; Sáo et al., 2021) and is described in the references therein. Two samples of carbopol gel[1] were used as test-fluids and their rheological characterization was carried out using an R/S Brookfield rotational rheometer, also described in previous works (Minussi & Maciel, 2012; Pereira & Maciel, 2021; Pereira et al., 2022). In this work, eighteen (18) new results of steady uniform flows of carbopol gels are reported. Rheological characterization was executed using coaxial geometry with CC-45 spindles. The rheometry protocol consisted of imposing shear rate to the flow in two stages (an increasing phase from 0 to $100 s^{-1}$ for 200 seconds and a decreasing phase for 200 seconds) and measuring the resulting shear stress. The properties of the flow (channel slope and flow rate) and of the test-fluid (mass concentration, fluid rheology and density) are described in Subsection "Test scenarios".

Test scenarios

First, the hypothetical scenarios are described and then the experimental cases are reported. The scenarios are characterized by the channel slope θ, flow rate Q, consistency index K_n (viscosity μ in the Newtonian case), flow index n and dimensionless yield stress C^*. Theoretical normal depth h_{0T} was calculated by solving implicitly the Equation 3.

Hypothetical scenarios consisted of fluids characterized by different rheological models: Newtonian ($n = 1$ and $C^* = 0$), Power-Law ($n < 1$ and $C^* = 0$), Bingham ($n = 1$ and $C^* > 0$) and Herschel-Bulkley ($n < 1$ and $C^* > 0$). Flow index was limited to $0.1 \le n \le 1.0$ and dimensionless yield stress to $0 \le C^* \le 0.830$, where each property was selected almost in a uniform manner within each correspondent range. These are the relevant properties to calculate the values of shear rates (Equation 5) and cover almost entirely the physically possible ranges of n and C^*, i.e. pseudoplastic fluids present $0 < n < 1$ and the flow of viscoplastic fluids is only possible for $C^* < 1$. Fluid density was fixed as $1000\ kg\,m^{-3}$ and the channel slope was limited to $\theta < 4°$. Constant inlet flow rates ($0.2 \le Q \le 5.0\, L\,s^{-1}$) and consistency index ($0.01 \le K_n \le 40\, Pa.s^n$) were attributed in *ad hoc* manner in order to simulate flows with normal depths typical of prototype scales (up to $30 cm$) and relatively low Reynolds numbers ($Re_H < 700$, laminar regime). In total, one hundred and fifty nine (159) hypothetical scenarios were simulated and all data is available in the Supplementary Material in form of spreadsheet. All of the 159 hypothetical scenarios were simulated using the Lax-Friedrichs code, while 108 were simulated by HEC-RAS 6.3.

The experimental scenarios were based on the procedures described in Subsection "Experimental methods". The tests were carried out using different channel slopes of $4° \le \theta \le 10°$, flow rates of $0.2 \le Q \le 0.9\, L/s$ and fluid rheology (carbopol gels with 0.15% and 0.17% of mass concentration). Experimental results from previous works in literature (Haldenwang et al., 2010; Fiorot et al., 2015; Maciel et al., 2018) were used to complement the experimental dataset. Thirty-one (31) experimental scenarios (see Table A1 from Annex A) were simulated through LF_N and LF_{HB} models.

[1] Carbopol gel is a polymeric solution that presents non-Newtonian effects, such as viscoplasticity and pseudoplasticity. It is commonly used as test-fluid for controlled experiments.

For ANSYS Fluent simulations, Table 1 shows the input parameters and fluid characteristics. Since full-momentum simulations have expensive computational costs, four cases were simulated, one for each rheological model.

RESULTS AND DISCUSSION

From now on, the subscript "$_0$" from normal depth h_0 is dropped, so the nomenclature for normal depth is now "h". Initially, the Lax-Friedrichs numerical implementation is validated by comparing the results of the LF_N model (h_{LF_N}) with HEC-RAS 6.3 results (h_{RAS}). For that, the same Equation 11, that contains Equation 6, was used for both codes. Figure 1 shows the comparison in terms of normal depth h. It is clear that the LF_N model reproduces the HEC-RAS 6.3 results for any rheological model, since the same equation (Equation 11) for bottom friction is used. Thus, the Lax-Friedrichs scheme is considered to be implemented correctly. Now the LF scheme is validated, Equations 11 and 12 can be properly evaluated through LF_N and LF_{HB} models, respectively.

Figure 2 compares normal depth results obtained through LF_N and LF_{HB} models. Theoretical solution of each scenario (h_T) is used as reference, thus the normal depth of each scenario is normalized by the each correspondent theoretical normal depth. It is observed that the ratios of normal depth obtained by the LF_{HB} model to theoretical normal depth ($h_{LF_{HB}} / h_T$) are close to unity, indicating a good agreement between numerical and theoretical results. On the other hand, the ratios of normal depth obtained by the LF_N model to the theoretical normal depth (h_{LF_N} / h_T) are between 0.86 and 1.00. It means that the values of normal depth obtained by LF_N model can reach up to 14% deviation from the theoretical value.

The rheological model of each data point must be observed. The Newtonian model is very close to unity on both axis, which shows a good numerical-theoretical agreement for both numerical models. However, by evaluating other rheological models, the deviation in normal depth for the LF_N model becomes more significant. Although the three remaining rheological models have points in all range of deviation, from 0.86 to 1.00, it is noted that the Herschel-Bulkley model presents a cluster of higher-deviation points, around $h_{LF_N} / h_T = 0.88$.

To understand why the normal depths of Herschel-Bulkley fluid flows are more susceptible to deviation using the LF_N model, Figure 3 shows a theoretical analysis of the shear rate formulations of LF_N and LF_{HB} models in function of flow index n and dimensionless yield stress C^* for each scenario. It contains hypothetical data (please see Supplementary Material) and experimental data (please see Subsection "Experimental methods" and Annex A). The scattered points represent each scenario and show that a vast range of n and C^* was considered in the study. To construct the color map, the ratio of shear rates $\dot{\gamma}_{HB} / \dot{\gamma}_N$ was calculated using Equations 5 and 6. It is clear that the more pseudoplastic ($n < 1$) or more viscoplastic ($C^* > 0$) the fluid is, the higher is the ratio $\dot{\gamma}_{HB} / \dot{\gamma}_N$. If both effects are combined, such as the case of the Herschel-Bulkley rheological model, the ratio of

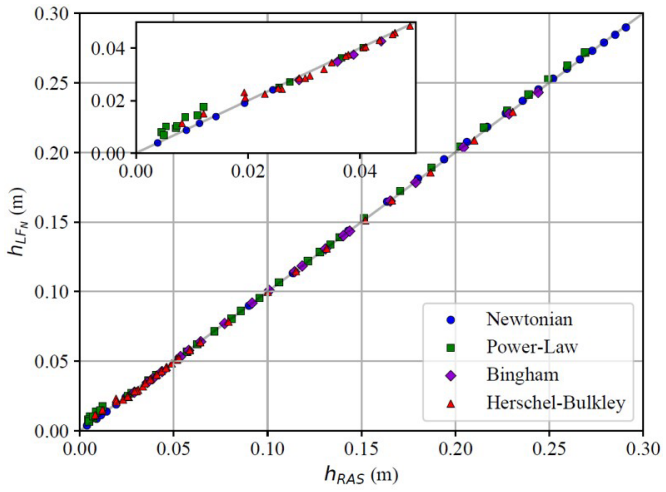

Figure 1. Comparison of normal depth results obtained by the LF_N and LF_{HB} models.

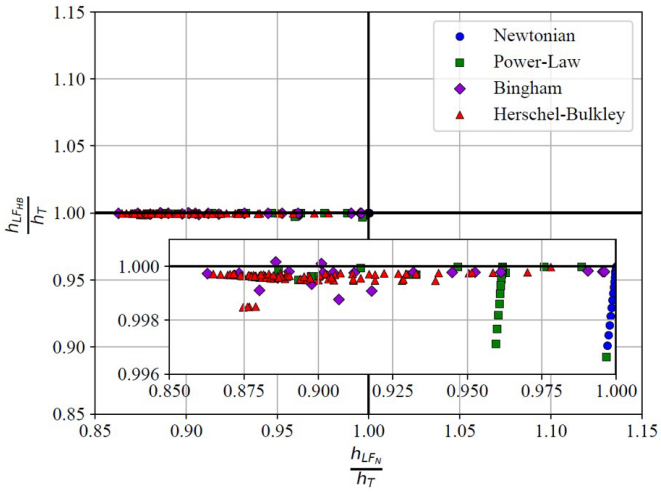

Figure 2. Comparison between normal depths obtained by LF_N and LF_{HB} models using theoretical solution as reference.

Table 1. Input parameters for ANSYS Fluent simulations. Cases 'N', 'PL', 'B' and 'HB' refer to Newtonian, Power-Law, Bingham and Herschel-Bulkley models, respectively.

Case	$\bar{U}\ (m\,s^{-1})$	$h_0\ (mm)$	$\theta\ (°)$	$\tau_c\ (Pa)$	$K_n\ (Pa\,s^n)$	$n\ (-)$	$\rho\ (kg\,m^{-3})$	$C^*\ (-)$
N	0.2558	9.83	8.00	0.00	0.212	1.000	1237.00	0.000
PL	0.2357	5.70	1.03	0.00	0.140	0.400	1120.00	0.000
B	0.0200	33.10	4.00	12.53	3.160	1.000	1000.00	0.553
HB	0.0220	29.83	4.00	11.13	4.260	0.430	1000.00	0.545

shear rates is sensibly affected. Such ratio can be understood as a deviation of the Herschel-Bulkley based shear rate (Equation 5) from the Newtonian-based shear rate (Equation 6). Since the only difference between models LF_N and LF_{HB} is the friction term, this analysis indicates that the deviation in normal depths presented by Figure 2 is linked to the deviation in shear rate.

To observe the influence of the shear rate deviation over the normal depth results, Figure 4 shows the relationship between ratios of normal depth (h_{LF_N}/h_T) and the ratios of shear rate ($\dot{\gamma}_{HB}/\dot{\gamma}_N$). It is clear that the deviation in normal depth is very sensitive to the deviation in shear rate, especially for $\dot{\gamma}_{HB}/\dot{\gamma}_N < 2.5$. The magnitude of their correlation can be quantified through the Spearman's rank correlation procedure (Zar, 1972). A Spearman correlation coefficient $r_s = -0.79$ is calculated from the 159 hypothetical simulated points. It shows a strong and monotonically decreasing correlation between both ratios. From this observation, it can be inferred that the deviation in normal depth is directly related to the shear rate formulation used by LF_N model (Equation 5). Even if the uncertainties in estimating rheological parameters could surpass the deviations in normal depth, this result means that using Equation 6 to model shear rates already yield these deviations even in hypothetical scenarios or very controlled experiments.

An inflection region can be observed in Figure 4 for $\dot{\gamma}_{HB}/\dot{\gamma}_N \approx 2.5$, where the monotonically decreasing behavior of h_{LF_N}/h_T changes to an increasing behavior. The points located at $\dot{\gamma}_{HB}/\dot{\gamma}_N > 2.5$ are scenarios where dimensionless yield stress C^* is high and/or flow index n is low, as Figure 3 indicates.

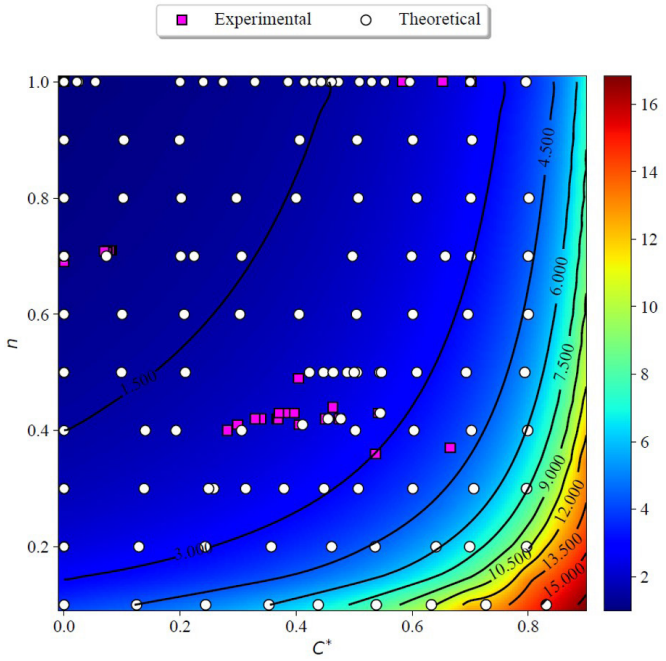

Figure 3. Ratio of shear rates $\dot{\gamma}_{HB}/\dot{\gamma}_N$ in function of dimensionless yield stress C^* and flow index n. Scattered points represent the hypothetical and experimental scenarios for every rheological model considered in the work. Newtonian fluids are represented by $C^* = 0$ and $n = 1$, Power-Law fluids by $C^* = 0$ and $n <$, Bingham fluids by $C^* > 0$ and $n = 1$, and Herschel-Bulkley fluids by $C^* > 0$ and $n < 1$.

For these scenarios, Equation 11 allows two analyses: 1) the contribution of yield stress τ_c surpasses significantly the contribution of the viscous term $K_n\dot{\gamma}^n$; or 2) lower flow indexes n reduce significantly the contribution of the viscous term $K_n\dot{\gamma}^n$. The combination of both analyses is also possible. Thus, these analyses mean that shear rate has less effect on the friction term for highly viscoplastic and/or pseudoplastic fluids, so the numerical normal depth is less affected by the shear rate deviation, as the tendency for $\dot{\gamma}_{HB}/\dot{\gamma}_N > 2.5$ indicates.

In terms of applicability in real events of mudflows, debris flows and tailings flows, it is important to estimate the order of magnitude of the shear rate within the flow. O'Brien & Julien (1988) report that typical shear rates for hyperconcentrated flows are on the order of $5 - 50\,s^{-1}$, while Major & Pierson (1992) state that open-channel debris flows rarely exceed $20\,s^{-1}$ and maintain rheometry measurements below $50\,s^{-1}$. Sosio & Crosta (2009) also agree that these events present shear rates on the order of $10 - 15\,s^{-1}$. Figure 4 shows the range of shear rate values for each scenario, stablishing three ranges of shear rate based on the discussed literature. The first range is $\dot{\gamma} \leq 20\,s^{-1}$, typical of these real events; the second range is $20 < \dot{\gamma} \leq 50\,s^{-1}$, incorporating uncommon (however observable) values of shear rates; and the third range is $\dot{\gamma} > 50\,s^{-1}$ for very uncommon values. From Figure 4, it is clear that most of scenarios from the first and second ranges are located at $\dot{\gamma}_{HB}/\dot{\gamma}_N \approx 2.5$, where most of the deviation occur. This observation means that the usage of the Newtonian-based shear rate (Equation 6) instead of the Herschel-Bulkley based shear rate (Equation 5) would provide higher deviations in situations typical of real-event flows.

Finally, Table 2 shows results of normal depth and bottom shear rate of simulations carried out by ANSYS Fluent 14.5. Solutions of the LF_{HB} model are used as reference to calculate the deviation in normal depth (ϵ_h) and in bottom shear rate ($\epsilon_{\dot{\gamma}_b}$), where both present low errors and, consequently, good numerical-theoretical agreement.

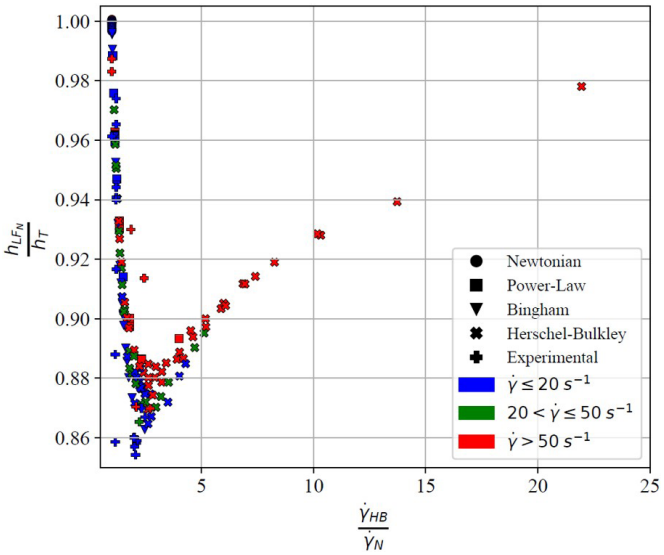

Figure 4. Relationship between ratios of normal depth (h_{LF_N}/h_T) and the ratios of shear rate ($\dot{\gamma}_{HB}/\dot{\gamma}_N$). For experimental data, the reference is given by the experimental normal depth, so the ratio becomes h_{LF_N}/h_{exp}. Shear rate values ($\dot{\gamma}$) are calculated through Equation 5.

Table 2. Results of ANSYS Fluent simulations in terms of deviation in normal depth and in bottom shear rate from theoretical solution.

Case	ϵ_h (%)	$\epsilon_{\dot{\gamma}_b}$ (%)
Newtonian	0.20	0.37
Power-Law	1.40	1.47
Bingham	1.07	0.17
Herschel-Bulkley	1.94	0.67

Full-momentum CFD codes calculate bottom shear rate through the complete velocity field (see Equation 15), without the shallow-water hypothesis made by the LF models. Since a good agreement with theoretical shear rate (Equation 15) is obtained for any rheological model studied in this work, these results corroborate the usage of Equation 12, and consequently Equation 5, in the friction term of SWE models. In this particular study, using SWE models is more advantageous than using CFD codes due to a significant difference in computational cost (order of minutes to SWE solvers and hours to CFD solvers) and to the obtainment of, virtually, the same solution.

CONCLUSIONS

This work explored the steady uniform flow as a theoretical reference to investigate two equations of shear rate (Equations 5 and 6) applied to the Shallow-Water Equations system. Three numerical codes were used (Lax-Friedrichs finite difference scheme, HEC-RAS 6.3 and ANSYS Fluent 14.5) and experimental data were gathered to confront with theoretical solutions. Extensive simulations using the Lax-Friedrichs scheme were performed, employing four rheological models (Newtonian, Power-Law, Bingham and Herschel-Bulkley) and different conditions of laminar flows. For hypothetical scenarios, it was shown that the shear rate formulation based on the Herschel-Bulkley model (Equation 5) presented good numerical-theoretical confrontation results, corroborated by the four simulations carried out by ANSYS Fluent 14.5. On the other hand, the Newtonian-based shear rate formulation (Equation 6) deviated from theoretical solution by 14% at maximum on a shear rate range typical of real-event flows. A strong and monotonically decreasing correlation (Spearman rank's correlation $r_s = -0.79$) was found between the ratio of shear rates and the ratio of normal depths, indicating that the formulation of Equation 11 is directly linked to the normal depth deviation from theoretical solution. Thus, for idealized cohesive mudflows, it is shown that a shear rate formulation based on a non-Newtonian model (Equation 5) performs better than the Newtonian-based shear rate approach (Equation 6) applied in most models. The steady uniform condition was evaluated in this work and further studies should be carried out for non-steady and non-uniform flows of non-Newtonian fluids.

ACKNOWLEDGEMENTS

The authors would like to thank FAPESP – Fundação de Amparo à Pesquisa do Estado de São Paulo (2020/07822-0 and 2022/05184-1) and CAPES – Coordenação de Aperfeiçoamento de Pessoal de Nível Superior (88887.640433/2021-00) for providing the financial support for this research.

REFERENCES

Ancey, C., Andreini, N., & Epely-Chauvin, G. (2012). Viscoplastic dambreak waves: review of simple computational approaches and comparison with experiments. *Advances in Water Resources*, *48*, 79-91.

ANSYS Fluent. (2012). *ANSYS Fluent 14.5 user's guide*. Canonsburg: ANSYS Inc.

Balmforth, N. J., Craster, R. V., Perona, P., Rust, A. C., & Sassi, R. (2007). Viscoplastic dam breaks and the bostwick consistometer. *Journal of Non-Newtonian Fluid Mechanics*, *142*(1), 63-78.

Boutounet, M., Monnier, J., & Vila, J.-P. (2016). Multi-regime shallow free surface laminar flow models for quasi-newtonian fluids. *European Journal of Mechanics - B/Fluids*, *55*, 182-206.

Castro-Orgaz, O., & Hager, W. H. (2019). *Shallow water hydraulics*. Cham: Springer.

Celik, I. B., Ghia, U., Roache, P. J., & Freitas, C. J. (2008). Procedure for estimation and reporting of uncertainty due to discretization in cfd applications. *Journal of Fluids Engineering-Transactions of the ASME*, *130*(7), 1-4.

Coussot, P. (1994). Steady, laminar, flow of concentrated mud suspensions in open channel. *Journal of Hydraulic Research*, *32*(4), 535-559.

Coussot, P. (2017). *Mudflow rheology and dynamics*. Abingdon: Routledge.

Coussot, P., & Meunier, M. (1996). Recognition, classification and mechanical description of debris flows. *Earth-Science Reviews*, *40*(3-4), 209-227.

Coussot, P., & Piau, J. M. (1994). On the behavior of fine mud suspensions. *Rheologica Acta*, *33*(3), 175-184.

Coussot, P., Laigle, D., Arattano, M., Deganutti, A., & Marchi, L. (1998). Direct determination of rheological characteristics of debris flow. *Journal of Hydraulic Engineering*, *124*(8), 865-868.

Di Cristo, C., Iervolino, M., & Vacca, A. (2013). Waves dynamics in a linearized mud-flow shallow model. *Applied Mathematical Sciences*, *7*(8), 377-393.

Fiorot, G. H., Maciel, G. F., Cunha, E. F., & Kitano, C. (2015). Experimental setup for measuring roll waves on laminar open channel flows. *Flow Measurement and Instrumentation*, *41*, 149-157.

Fraccarollo, L., & Toro, E. F. (1995). Experimental and numerical assessment of the shallow water model for two-dimensional dam-break type problems. *Journal of Hydraulic Research*, *33*(6), 843-864.

Gama, I. R. V., Simões, A. L. A., Schulz, H. E., & Porto, R. M. (2020). Código livre para solução numérica das equações de Saint-Venant em canais trapezoidais assimétricos. *Revista Eletrônica de Gestão e Tecnologias Ambientais*, *8*(2), 145-159.

Garcia-Navarro, P., Alcrudo, F., & Saviron, J. M. (1992). 1-D open-channel flow simulation using TVD-McCormack scheme. *Journal of Hydraulic Engineering*, *118*(10), 1359-1372.

Gibson, S., Floyd, I., Sánchez, A., & Heath, R. (2021). Comparing single-phase, non-newtonian approaches with experimental results: validating flume-scale mud and debris flow in HEC-RAS. *Earth Surface Processes and Landforms*, *46*(3), 540-553.

Gibson, S., Moura, L. Z., Ackerman, C., Ortman, N., Amorim, R., Floyd, I., Eom, M., Creech, C., & Sánchez, A. (2022). Prototype scale evaluation of non-Newtonian algorithms in HEC-RAS: mud and debris flow case studies of Santa Barbara and Brumadinho. *Geosciences*, *12*(3), 134-134.

Gildeh, H. K., Halliday, A., Arenas, A., & Zhang, H. (2021). Tailings dam breach analysis: A review of methods, practices, and uncertainties. *Mine Water and the Environment*, *40*(1), 128-150.

Haldenwang, R., Kotzé, R., & Chhabra, R. (2012). Determining the viscous behavior of non-Newtonian fluids in a flume using a laminar sheet flow model and Ultrasonic Velocity Profiling (UVP) system. *Journal of the Brazilian Society of Mechanical Sciences and Engineering*, *34*, 276-284.

Haldenwang, R., Slatter, P. T., & Chhabra, R. P. (2010). An experimental study of non-Newtonian fluid flow in rectangular flumes in laminar, transition and turbulent flow regimes. *Journal of the South African Institution of Civil Engineering*, *52*(1), 11-19.

Hicks, F. E., & Peacock, T. (2005). Suitability of HEC-RAS for flood forecasting. *Canadian Water Resources Journal*, *30*(2), 159-174.

Hirt, C. W., & Nichols, B. D. (1981). Volume of fluid (vof) method for the dynamics of free boundaries. *Journal of Computational Physics*, *39*(1), 201-225.

Hu, K., Mingham, C. G., Clive, G., & Causon, D. M. (2000). Numerical simulation of wave overtopping of coastal structures using the non-linear shallow water equations. *Coastal Engineering*, *41*(4), 433-465.

Huang, X., & Garcia, M. H. (1998). A Herschel–Bulkley model for mud flow down a slope. *Journal of Fluid Mechanics*, *374*, 305-333.

Iverson, R. M. (1997). The physics of debris flows. *Reviews of Geophysics*, *35*(3), 245-296.

Jeyapalan, J. K., Duncan, J. M., & Seed, H. B. (1983). Analyses of flow failures of mine tailings dams. *Journal of Geotechnical Engineering*, *109*(2), 150-171.

Jing, L., Kwok, C. Y., Leung, Y. F., Zhang, Z., & Dai, L. (2018). Runout scaling and deposit morphology of rapid mudflows. *Journal of Geophysical Research. Earth Surface*, *123*(8), 2004-2023.

Liang, D., Falconer, R. A., & Lin, B. (2006). Comparison between TVD-MacCormack and ADI-type solvers of the shallow water equations. *Advances in Water Resources*, *29*(12), 1833-1845.

Maciel, G. F., Cunha, E. F., Sao, Y. T., Toniati, A. L., Fiorot, G. H., Ferreira, F. O., Kitano, C., & Gonçalves Junior, V. P. (2018). Non-intrusive techniques to measure roll waves level evolving in a flume. *E3S Web of Conferences*, *40*, 05049.

Maciel, G. F., Ferreira, F. O., & Fiorot, G. H. (2013). Control of instabilities in non-newtonian free surface fluid flows. *Journal of the Brazilian Society of Mechanical Sciences*, *35*(3), 217-229.

Maciel, G. F., Ferreira, F. O., Cunha, E. F., & Fiorot, G. H. (2017). Experimental apparatus for roll-wave measurements and comparison with a 1D mathematical model. *Journal of Hydraulic Engineering*, *143*(11), 04017046.

Major, J. J., & Pierson, T. C. (1992). Debris flow rheology: experimental analysis of fine-grained slurries. *Water Resources Research*, *28*(3), 841-857.

Martin, V., Al-Mamun, M., & Small, A. (2019). CDA technical bulletin on tailings dam breach analyses. In J. P. Tournier, T. Bennett & J. Bibeau (Eds.), *Sustainable and Safe Dams Around the World (Vol. 1). Proceedings of the ICOLD 2019 Symposium, (ICOLD 2019)* (pp. 3484-3499). Boca Raton: CRC Press. https://doi.org/10.1201/9780429319778.

Minussi, R. B., & Maciel, G. F. (2012). Numerical experimental comparison of dam break flows with non-Newtonian fluids. *Journal of the Brazilian Society of Mechanical Sciences and Engineering*, *34*, 167-178.

Ng, C.-O., & Mei, C. C. (1994). Roll waves on a shallow layer of mud modelled as a power-law fluid. *Journal of Fluid Mechanics*, *263*, 151-184.

O'Brien, J. S., & Julien, P. Y. (1988). Laboratory analysis of mudflow properties. *Journal of Hydraulic Engineering*, *114*(8), 877-887.

O'Brien, J. S., Julien, P. Y., & Fullerton, W. T. (1993). Two-dimensional water flood and mudflow simulation. *Journal of Hydraulic Engineering*, *119*(2), 244-261.

Paiva, C. A., Santiago, A. F., & Prado Filho, J. F. (2020). Content analysis of dam break studies for tailings dams with high damage potential in the Quadrilátero Ferrífero, Minas Gerais: technical weaknesses and proposals for improvements. *Natural Hazards*, *104*(2), 1141-1156.

Pereira, J. B., & Maciel, G. F. (2021). Automated slump test: an effective alternative in predicting rheological properties and an efficient tool for providing the quality control of materials. *Measurement*, *178*, 109384.

Pereira, J. B., Sáo, Y. T., & Maciel, G. F. (2022). Numerical and experimental application of the automated slump test for yield stress evaluation of mineralogical and polymeric materials. *Rheologica Acta*, *61*(2), 163-182.

Sáo, Y. T., Pereira, J. B., Fiorot, G. H., & Maciel, G. F. (2021). Obtaining flow curve for viscoplastic fluids through inclined open-channel apparatus. *Journal of the Brazilian Society of Mechanical Sciences and Engineering*, *43*(5), 278.

Sosio, R., & Crosta, G. B. (2009). Rheology of concentrated granular suspensions and possible implications for debris flow modeling. *Water Resources Research*, *45*(3), W03412.

Tan, W.-Y. (1992). *Shallow water hydrodynamics: mathematical theory and numerical solution for a two-dimensional system of shallow-water equations*. Amsterdam: Elsevier.

Tsakiris, G., & Bellos, V. (2014). A numerical model for two-dimensional flood routing in complex terrains. *Water Resources Management*, *28*, 1277-1291.

US Army Corps of Engineers. (2020). *HEC-RAS 6.3 guides and tutorials*. Davis: US Army Corps of Engineers/Hydrologic Engineering Center.

US Army Corps of Engineers. (2022). *HEC-RAS 6.3 hydraulic reference manual*. Davis: US Army Corps of Engineers/Hydrologic Engineering Center.

Van Leer, B. (1979). Towards the ultimate conservative difference scheme. V. A second-order sequel to Godunov's method. *Journal of Computational Physics*, *32*(1), 101-136.

Wu, Y.-H., Liu, K.-F., & Chen, Y.-C. (2013). Comparison between FLO-2D and Debris-2D on the application of assessment of granular debris flow hazards with case study. *Journal of Mountain Science*, *10*, 293-304.

Yi, X. (2011). A dam break analysis using HEC-RAS. *Journal of Water Resource and Protection*, *3*(6), 5707.

Zar, J. H. (1972). Significance testing of the spearman rank correlation coefficient. *Journal of the American Statistical Association*, *67*(339), 578-580.

Authors contributions

Yuri Taglieri Sáo: Proposed the research problem, carried out numerical simulations and further comparisons, analysed the results, prepared figures for data visualization, wrote the first draft of the manuscript, and approved the final version of the manuscript.

João Batista Pereira: Carried out experiments and further comparisons, analysed the results, and approved the final version of the manuscript.

Geraldo de Freitas Maciel: Proposed the research problem, analysed the results, reviewed the first draft of the manuscript, and approved the final version of the manuscript.

Editor-in-Chief: Adilson Pinheiro
Associated Editor: Iran Eduardo Lima Neto

ANNEX A. TABLE A1 PRESENTS RHEOMETRY DATA AND EXPERIMENTAL DATA FROM STEADY UNIFORM FLOWS IN RECTANGULAR AND INCLINED CHANNELS.

Table A1. Properties of each experimental scenario.

	$\tau_c\ (Pa)$	$K_n\ (Pa.s^n)$	$n\ (-)$	$\rho\ (Kg\,m^{-3})$	$Q\ (L\,s^{-1})$	$\theta\ (°)$	$h_{exp}\ (m)$	$C^*\ (-)$
Experimental obtained in this work	11.13	4.26	0.43	1000.00	0.2	4	0.0300	0.542
	11.04	4.74	0.42	1000.67	0.61	4	0.0340	0.475
	11.26	5.05	0.42	999.33	0.41	4	0.0366	0.450
	10.75	5.32	0.41	1000.67	0.87	4	0.0388	0.405
	10.87	4.47	0.44	1000.67	0.23	6	0.0229	0.463
	10.61	4.24	0.49	998.67	0.41	6	0.0256	0.404
	10.71	4.72	0.43	998.67	0.63	6	0.0274	0.382
	10.83	5.09	0.42	1001.33	0.83	6	0.0288	0.367
	11.54	5.03	0.42	1000.67	0.21	8	0.0229	0.369
	11.62	5.08	0.42	999.33	0.42	8	0.0256	0.332
	11.17	5.64	0.41	996.67	0.6	8	0.0274	0.299
	11.05	5.93	0.4	1000.00	0.76	8	0.0288	0.281
	11.09	4.81	0.43	999.33	0.21	10	0.0164	0.397
	11.72	4.76	0.43	1000.67	0.41	10	0.0186	0.370
	11.56	5.1	0.42	1000.67	0.6	10	0.0200	0.339
	11.78	5.21	0.42	999.33	0.75	10	0.0210	0.329
	32.49	12.94	0.37	1001.93	0.39	8	0.0358	0.665
	32.88	19.93	0.36	1001.93	0.75	8	0.0449	0.537
Maciel et al. (2018)	0.40	0.171	0.71	1020.00	0.22	5	0.0055	0.082
	0.40	0.172	0.71	1020.00	0.27	5	0.0057	0.080
	0.40	0.172	0.71	1020.00	0.32	5	0.0058	0.079
	0.40	0.176	0.71	1020.00	0.36	5	0.0061	0.075
	0.40	0.165	0.71	1020.00	0.41	5	0.0063	0.072
	0.40	0.169	0.71	1020.00	0.46	5	0.0066	0.069
Haldenwang et al. (2012)	0.00	0.92	0.69	1030.00	2.78	1	0.0438	0.000
	0.00	0.92	0.69	1030.00	6.79	1	0.0587	0.000
	2.80	0.008	1.00	1032.00	3.12	1	0.0226	0.701
	2.80	0.008	1.00	1032.00	4.36	1	0.0243	0.652
	2.80	0.008	1.00	1032.00	3.27	2	0.0136	0.583
Fiorot et al. (2015)	0.00	0.2111	1.00	1273.00	0.75	8	0.0098	0.000
	0.00	0.2173	1.00	1273.00	0.96	8	0.0107	0.000
	0.00	0.2117	1.00	1273.00	1.14	8	0.0116	0.000

SUPPLEMENTARY MATERIAL

Supplementary material accompanies this paper.

Data used for numerical simulations are available in form of spreadsheet in the following URL: https://osf.io/nuz7s/?view_only=6335043427ec4aeaa358f7812091c781